European Journal of Chemistry

View Journal Online
View Article Online

Synthesis, photochromic, and electrochromic properties of a Schiff-base pyrazolone: An experimental and theoretical study

Pratima Surati

Department of Chemistry, M. B. Patel Science College, Sardar Patel University, Anand-388001, Gujarat, India

** Corresponding author at: Department of Chemistry, M. B. Patel Science College, Sardar Patel University, Anand-388001, Gujarat, India.*
e-mail: prsurati21@gmail.com (P. Surati).

RESEARCH ARTICLE

10.5155/eurjchem.17.2.138-145.2750

Received:25 December 2025
Received in revised form: 20 February 2026
Accepted: 10 April 2026
Published online: 30 June 2026
Printed: 30 June 2026

KEYWORDS

Schiff base
Pyrazolone
Photochromic
Electrochromic
Theoretical study
Photoisomerization

ABSTRACT

Schiff-base pyrazolone derivatives have garnered significant attention due to their intriguing photochromic and electrochromic properties, which hold promise for applications in molecular switches, sensors, and advanced optical materials. Schiff base, 5-methyl-2-phenyl-4-(phenyl-*o*-tolylamino-methylene)-2,4-dihydropyrazol-3-one (PMBP-2A1MB), was synthesized and characterized by means of NMR, IR, LC-MS, and UV-Vis absorption spectra. This research paper aims to dive into the synthesis and photochromic and electrochromic properties of Schiff base pyrazolone derivative. The photochromic study was investigated using 365 and 430 nm light and shows good results. The electrochromic study was conducted using a cyclic voltammetry study, which demonstrates quasi-reversibility in nature. Theoretical calculations were performed using geometries optimized at the B3LYP/6-31G(d,p) level of theory. By integrating these aspects, we seek to enhance the understanding of photoisomerization and structure-property relationships.

Cite this: *Eur. J. Chem.* **2026**, *17(2)*, 138-145 **Journal website**: www.eurjchem.com

1. Introduction

Photochromic and electrochromic materials exhibit reversible color changes under light irradiation or applied electric potential, making them attractive for applications in optical switching, smart windows, sensors, and display technologies. Organic chromophores are particularly appealing in this field because of their structural tunability, low cost, and fast response times. Schiff bases represent an important class of organic materials due to their simple synthesis, extended π-conjugation, and favorable charge transfer characteristics [1]. Incorporation of heterocyclic units into Schiff base frameworks often improves their optical and electrochemical properties [2]. Among these, pyrazolone-based Schiff bases have gained attention due to their rich tautomerism [3], strong donor-acceptor nature [4], and notable photoresponse behavior. Photochromism in Schiff bases is commonly associated with processes such as cis-trans isomerization, keto-enol tautomerism, or intramolecular proton transfer, which induce significant changes in electronic absorption spectra upon light irradiation [5].

Electrochromic behavior, on the other hand, originates from reversible redox processes that alter the electronic structure of the molecule, resulting in distinct optical transitions. As one of the most important applications, electrochromic materials are expected to save energy and improve living comfort. To date, they have been attracting research attention around the world, and the corresponding commercialization is continuously progressing [6-8]. Density functional theory (DFT), developed by pioneers such as Walter Kohn and John Pople, plays a vital role in interpreting photochromic and electrochromic responses by providing information on molecular geometry, electronic structure, frontier molecular orbitals, and electronic transitions [9].

Although several pyrazolone-based Schiff bases have been reported, most studies have focused mainly on synthesis, structural characterization, or biological activity, with limited attention to their combined photochromic, electrochromic, and theoretical electronic properties. In particular, the effect of substituted aromatic amine groups on the electronic structure, charge transfer, and chromic performance is still not explored sufficiently. Such structural modifications are expected to enhance π-electron delocalization and intramolecular charge transfer, thus improving optical and redox behavior. Therefore, systematic investigation of structurally modified derivatives is essential to establish clear structure-property relationships and improve chromic performance.

In this study, a new Schiff base (PMBP-2A1MB) containing a substituted aromatic amine moiety was synthesized and its photochromic and electrochromic properties were systema-

ISSN 2153-2249 (Print) / ISSN 2153-2257 (Online)
https://dx.doi.org/10.5155/eurjchem.17.2.138-145.2750

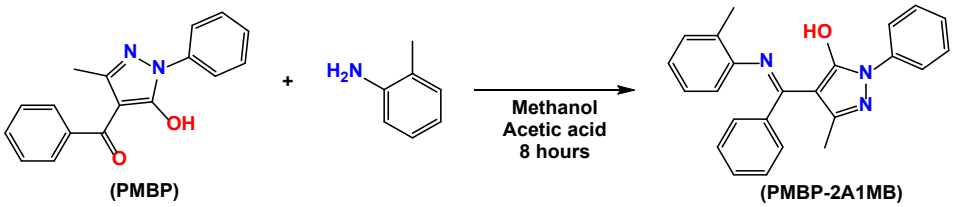

Scheme 1. Synthesis of 5-methyl-2-phenyl-4-(phenyl-o-tolylamino-methylene)-2, 4-dihydro-pyrazol-3-one.

tically investigated. The structural modification enhances conjugation and electronic communication, distinguishing it from previously reported analogues. Experimental results, supported by DFT calculations, provide insight into the relationship between the molecular structure and chromic behavior, contributing to the rational design of efficient pyrazolone-based chromic materials for optoelectronic applications.

2. Experimental

2.1. Measurement

2.1.1. Photochromic study

The sample is exposed to a 15 W Hitachi UV lamp with a 365 nm (longer UV) wavelength intensity. For the decolorization investigation, a 15 W (Philips) visible light lamp is used. The photochromic investigation was carried out in the solid state using a Hitachi UV-3010 spectrophotometer.

2.1.2. Cyclic voltammetry

A CH Instruments, Inc., Austin, TX, CHI600E Electrochemical Analyzer was used for the Cyclic Voltammetry (CV) investigation. Ag/Ag^+, platinum wire, and platinum disk were utilized as the reference, counter, and working electrodes, respectively. The required analyte concentrations were produced in acetonitrile (>99%, Sigma-Aldrich), and the supporting electrolyte was 0.1 M *tetra*-butyl ammonium hexafluorophosphate (TBAPF6) (>99%, Sigma-Aldrich). A voltage scan rate of 25 mV/s signal was applied to the run cycle as a function of time, with the applied potential being between -1.5 and 1.5 V. The internal standard utilized was ferrocene, and potentials with respect to the Fc/Fc^+ redox pair are displayed. Pick picking was done in the CorrView software, and standard redox potentials for analytes and the ferrocene/ferrocenium redox pair were computed from the CV.

2.1.3. Computational details

The optimized structure of 5-methyl-2-phenyl-4-(phenyl-*o*-tolylamino-methylene)-2,4-dihydro-pyrazol-3-one was obtained using the Gaussian 09 program [10] using the B3LYP functional. The 6-31G(d,p) basis set was employed in all calculations Geometry optimizations were performed in the methanol and gas phases. The polarizable continuum model (PCM) was used to model the methanol solvent environment. To verify that the optimized structures correspond to real minima, as shown by the lack of imaginary frequencies, frequency calculations were performed at the same theoretical level. The electronic and spectral characteristics were further analyzed using the improved geometrical parameters acquired.

2.2. Synthesis and characterization

The synthesis of the compound was carried out by reaction between 2-amine 1-methyl benzene and 4-benzoyl-5-methyl-2-phenyl-2,4-dihydro-3*H*-pyrazol-3-one (PMBP). PMBP synthesized according to the literature [12-14]. Take 250 mL flat bottom flask, add 50 mL of methanol and biketone (0.05 mmol) and warm untill dissolution. Take amine (0.05 mmol) in another beaker and dissolved in 30 mL of methanol, then add the amine solution in biketone solution, add a few drops of acetic acid (~0.5 mL) and stir the reaction mixture on a magnetic stirrer for 8 hours (scheme 1) [15,16].

5-Methyl-2-phenyl-4-(phenyl-o-tolylamino-methylene)-2, 4-dihydro-pyrazol-3-one: Color: Yellow. Yield: 79.23 %. M.p.: 176-178 °C. FT-IR (KBr, ν, cm^{-1}): 3060 (C-H, phenyl), 1672 (C=O), 1620 (C=N Schiff base), 1572 (C=Ncyclic), 1497, 1437 (phenyl), 1427, 1366 (pyrazolone ring). ^1H NMR (400 MHz, DMSO-d_6, δ, ppm): 2.26 (s, 3H, CH_3), 2.44 (s, 3H, CH_3), 7.30-7.90 (m, 14H, 2Ph, CH_3-Ph), 12.4 (d, 1H, N-H, J = 12.4 Hz). ^{13}C NMR (100 MHz, $CDCl_3$, δ, ppm): 165.17 (C=N, imine), 152.48 (C–OH), 149.02, 144.60, 141.84, 139.67 (Cq, aromatic and heterocyclic carbons), 131.82, 131.47, 129.21, 128.66, 124.93, 123.54, 121.36, 118.82, 118.11 (Ar-CH), 103.55 (C-4, pyrazolone ring), 13.15 (CH_3). MS (EI, *m/z* (%)): 368.42 (M+1) / 367.45. Anal. calcd. for $C_{24}H_{21}N_3O$: C, 78.45; H, 5.76; N, 11.44%. Found: C, 77.71; H, 5.73; N, 11.50%. UV/Vis ($CHCl_3$, λ_{max}, nm, (ε)): 210 (1.72×10^3), 250 (1.01×10^3), 345 (1.21×10^3). n^D25 = 1.626.

3. Results and discussions

3.1. Photochromic study

Figure 1 illustrates the temporal evolution of the UV-VIS spectra for 5-methyl-2-phenyl-4-(phenyl-*o*-tolylamino-methylene)-2,4-dihydro-pyrazol-3-one. Upon exposure to ultraviolet light at a wavelength of 365 nm and under ambient temperature conditions, the compound exhibited a transition in color from yellow to a deeper shade of dark yellow. The spectra were meticulously recorded at various time intervals until the spectral variation ceased to be discernible. Upon irradiation, the spectra revealed the emergence of a new band within the range of 380 to 425 nm, with its intensity progressively increasing as the measurements were performed. The phenomenon of photoinduced proton transfer between moieties is particularly intriguing, as the transition from the *enol* form to the *keto* form, coupled with the configurational rearrangement of the π-electrons, results in significant spectral alterations [17].

The photochromic reversibility of the compound was investigated by monitoring the absorbance at 401 nm over multiple irradiation cycles. Figure 2 shows the five cycles of the reversibility of photoirradiation process. The absorbance showed consistent and reversible switching between low and high values upon alternate irradiation, confirming efficient photoinduced transformation and recovery. The nearly identical response over five cycles indicates good reversibility, photostability, and fatigue resistance of the compound [18,19].

The kinetic curve (Figure 3) is plotted according to Equation 1.

$$\ln[A_\infty - A_0/A_\infty - A_t] = kt \quad (1)$$

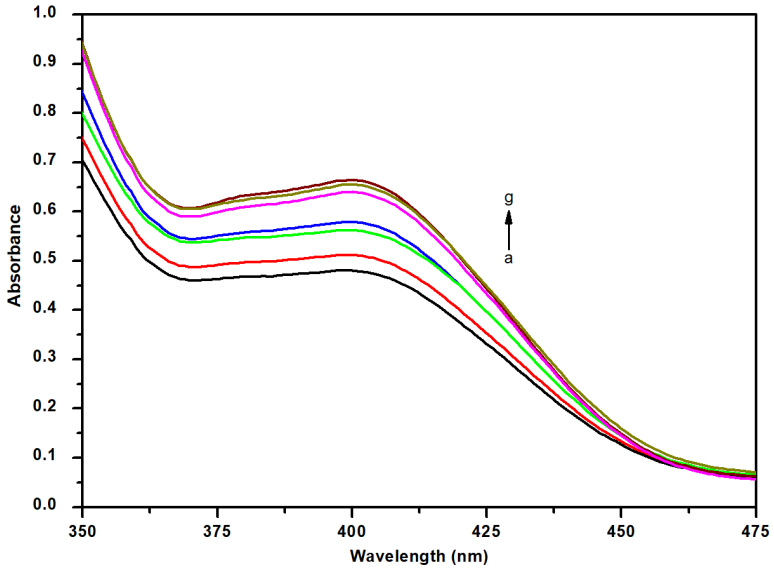

Figure 1. UV-vis absorption spectra in the solid state recorded at different irradiation times (0,10, 20, 30, 40, 50, 60 min, a–g).

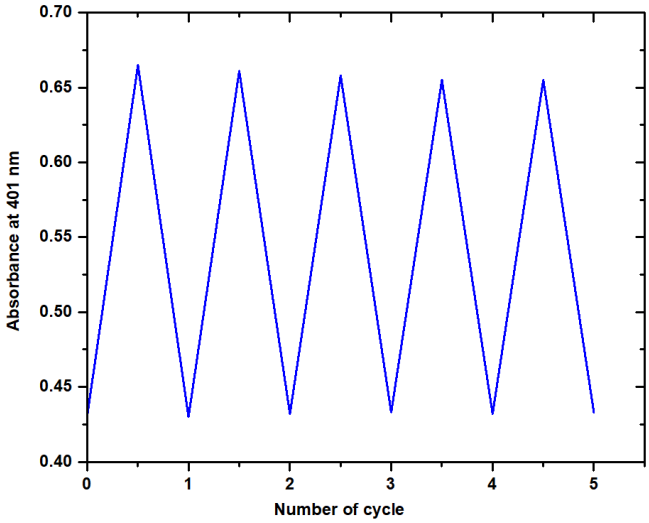

Figure 2. Reversible photochromic switching behavior of PMBP-2A1MB at 401 nm over five irradiation cycles.

where k is the first-order rate constant. A_0, A_∞ and A_t are the observed reflection data corresponding to the 410 nm wavelength at the beginning, end and time t of the reaction, follow well the pseudo-first order kinetics [20,21].

The dynamic UV-Vis spectral data were obtained from a single continuous measurement performed under controlled experimental conditions. The coefficient of determination (R^2) value of 0.8907 indicates a good correlation between the experimental data and the fitted curve (Figure 3). This confirms that the applied fitting model adequately describes the photochromic behavior of the compound. The slight deviation from an ideal fit may be attributed to experimental limitations and the dynamic nature of the photoisomerization process, which involves transient [22,23].

3.2. Electrochromic study

The cyclic voltammogram shows the variation of current with applied potential in the range of −1.3 V to +1.3 V. The anodic scan exhibits a gradual increase in current, with the oxidation onset potential (E_{onset}) observed at 0.768 V, indicating the initiation of the oxidation process. At higher positive potentials, the current increases further, confirming the electroactive nature of the compound [24]. The reverse scan shows a reduction response without a well-defined corresponding cathodic peak, suggesting a quasireversible electrochemical process. This result confirms the good electrochemical stability and provides a basis for estimating its HOMO energy level. The HOMO and LUMO levels unfold as a result of intermolecular interactions in organic materials with conjugation systems [25]. This unfolding is caused by narrow bands that comprise energetic levels known as the "band gap" (of organic semiconductors, which function similarly to the band gap of inorganic compounds) and typically range from 1 to 4 eV, which corresponds to the minimum energy required to generate an exited state [26,27].

Due to an increase in the electrical system, this bandgap typically decreases as the delocalization grows. A study using cyclic voltammetry Figure 4 revealed that the chemical exhibited a quasi-reversible voltammogram. Using CV data, the band gap was determined to be 2.79 eV [28,29], as seen in Table 1.

Table 1. Cyclic voltammetry data and calculated electronic parameters of the compound.

E_{onset} (Oxidation)	HOMO (eV) *	LUMO (eV) **	Band gap (E_{gap}) (eV)
0.768	-5.868	-3.789	2.79

* The HOMO energy level was calculated using the following equation: $E_{HOMO} = -(E_{onset}$ *vs* $Fc^+/Fc + 5.1)$ eV.
** The LUMO energy level was calculated using the following equation: $E_{LUMO} = E_{HOMO} + E_{gap}$ eV.

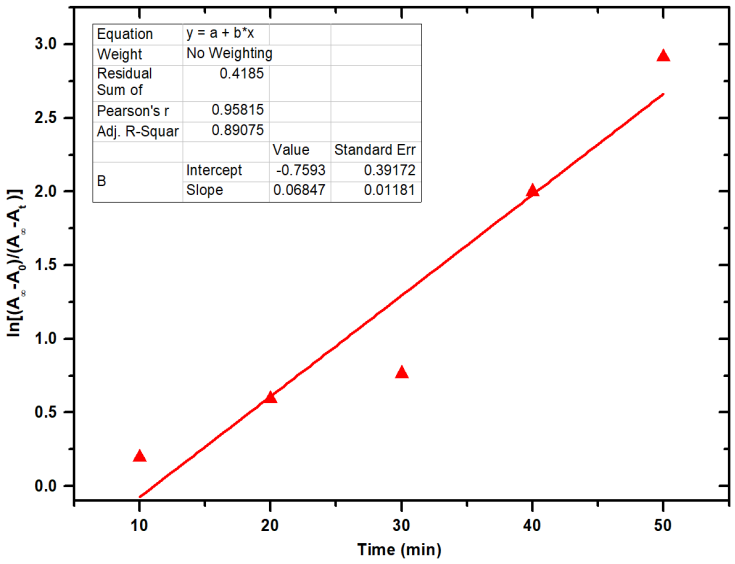

Figure 3. First-order kinetic plot for the photoisomerization reaction under 365 nm UV irradiation. Equation: y = a + bx; Pearson's r = 0.9518; intercept = −0.7594; slope = 0.06848.

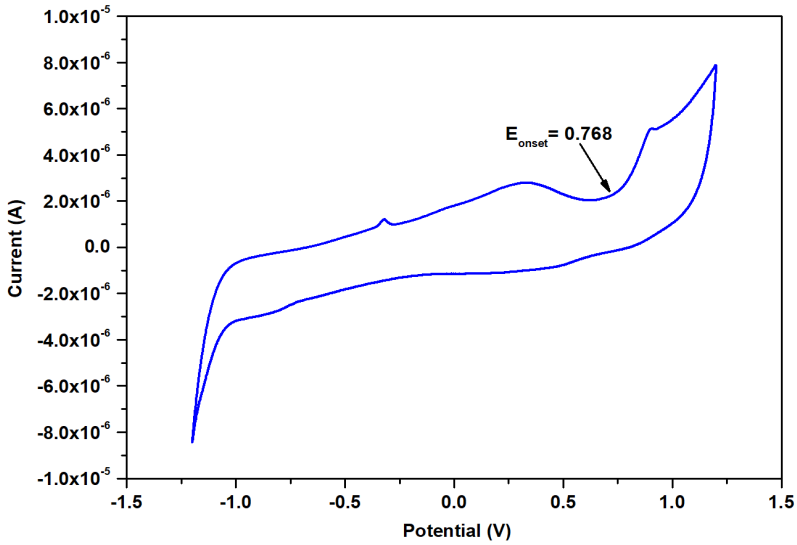

Figure 4. Cyclic voltammogram of PMBP-2A1MB recorded in acetonitrile at a scan rate of 25 mV/s.

The delocalization of electrons in molecules with respect to the band gap was further supported by evidence from cyclic voltammetry [30].

3.3. Theoretical study

Figure 5 shows two forms of the synthesized compound. The *keto* form (a) has zero relative stabilization energy compared to the *enol* form (b) with 29.13 kJ/mol. Compound with a lower relative energy (ΔE value) is generally more stable and less reactive than a compound with a higher relative energy.

The calculated electronic absorption spectrum of the *keto* form of the compound reveals three major electronic transitions in the UV-visible region. The low-energy absorption band observed at 485 nm corresponds to the HOMO → LUMO transition with a low oscillator strength (f = 0.0229), indicating a weakly allowed transition, likely associated with $n \rightarrow \pi^*$ or charge-transfer character [31]. A more intense absorption band appears at 357 nm, arising from the HOMO−2 → LUMO transition with the highest oscillator strength (f = 0.2228), suggesting a strongly allowed $\pi \rightarrow \pi^*$ transition and representing the dominant contribution to the absorption spectrum. Furthermore, an absorption band at 304 nm is attributed to the HOMO−4 → LUMO transition with moderate intensity (f = 0.0552). In general, the involvement of multiple occupied orbitals in these excitations reflects the presence of extended conjugation in the *keto* form, while the HOMO–LUMO

Table 2. Calculated electronic absorption spectra of the *keto* form of the compound.

Wavelength (nm)	Oscillator strength (*f*)	Electronic transition
485	0.0229	HOMO → LUMO
357	0.2228	HOMO-2 → LUMO
304	0.0552	HOMO-4 →LUMO

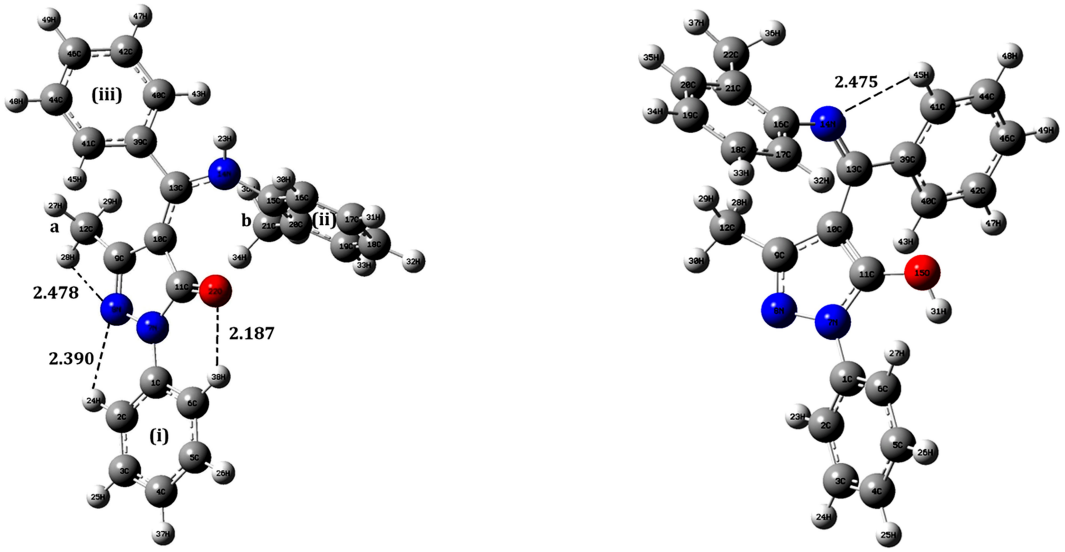

(a) (b)

Figure 5. B3LYP/6-31G(d,p)-optimized geometries of (a) *keto* and (b) *enol* tautomers of 5-methyl-2-phenyl-4-(phenyl-*o*-tolylaminomethylene)-2,4-dihydro-1*H*-pyrazol-3-one.

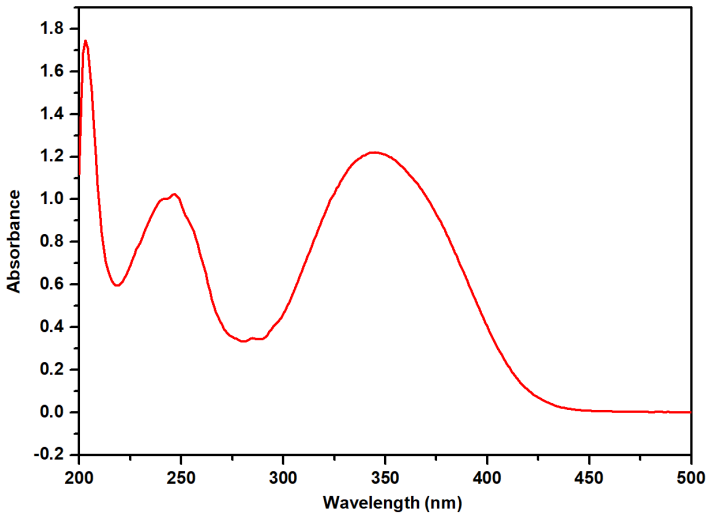

Figure 6. UV-vis absorption spectra of PMBP-2A1MB in methanol.

transition provides information on the electronic excitation energy and optical behavior of the compound [32]. The theoretical results agree well with the experimental data.

The experimental absorption maximum observed at 401 nm (380-425 nm region) shows a deviation from the calculated DFT value at 485 nm due to differences between experimental and theoretical conditions (Table 2). Theoretical calculations were performed in the gas phase, whereas the experimental spectrum was recorded in the solid state, where intermolecular interactions such as π–π stacking, hydrogen bonding and crystal packing can significantly alter orbital energies, resulting in a hypsochromic shift. Additionally, DFT calculations using conventional hybrid functionals often overestimate excitation wavelengths, particularly for π → π* and charge-transfer transitions, due to limitations in describing long-range electron correlation. The UV-vis spectra in solution is given in Figure 6. In solution, solvent effects play a significant role in stabilizing the ground and excited states differently, which alters the HOMO-LUMO energy gap and results in a shift of the absorption wavelength. In particular, solvent polarity and solute-solvent interactions tend to stabilize the excited state, leading to shifts in the observed absorption maxima compared to the theoretical predictions. Despite this quantitative difference, both experimental and theoretical results correspond to the same HOMO → LUMO transition, confirming the assignment of the validity of the electronic transition. Such deviations of 50-100 nm are commonly reported for conjugated Schiff base systems and are within the acceptable accuracy range of DFT methods [22,33].

Table 3. Calculated vibrational frequencies and their correlation with experimental FT-IR bands for the *enol* and *keto* forms, along with interpretation.

Calculated frequency (cm^{-1})	Enol form (cm^{-1})	Keto form (cm^{-1})	Interpretation
3452	3340	-	ν(O–H) stretching confirms the presence of the enol form; disappearance in keto indicates proton transfer
3452	-	- / weak	ν(N–H) stretching indicates the formation of keto tautomer after proton transfer
3135-3055	3060	3060	ν(C–H) aromatic stretching confirms aromatic ring present in both forms
3025-2929	2947	2947	ν(CH_3) stretching vibration unaffected by tautomerism
1682	-	1672	ν(C=O) stretching confirms formation of keto form
1600-1542	1659	-	ν(C=N) stretching confirms the azomethine group in enol form
1595-1548	-	1620	Shifted ν(C=N) due to electronic redistribution in keto form
1570	1572	1572	ν(C=C) aromatic stretching present in both forms
1548-1542	1543	1543	ν(C–N) stretching vibration present in both forms
1493	-	1497	N–H bending confirms formation of keto form
1471-1437	1458-1450	1458-1450	δ(CH_3) bending vibration present in both forms
1374-1344	1366-1344	1366-1344	Symmetric CH_3 bending vibration
1323	-	1323	ν(C–N) stretching supports keto structure formation
1278	1288	1278	ν(C–O) stretching in enol shifts due to keto formation
1134-1018	1173-1018	1173-1018	ν(C–O), ν(C–N) vibrations in fingerprint region
849-694	879-694	879-694	Aromatic C–H out-of-plane bending confirms substituted aromatic ring

Table 4. Selected bond lengths, bond angles, and hydrogen bond distances of the *keto* and *enol* tautomers of the compound. The corresponding parameters in methanol are given in parentheses.

Bond lengths (Å)	Keto	Enol
C_1-N_7	1.415 (1.412)	1.416 (1.421)
N_7-N_8	1.387 (1.393)	1.375 (1.377)
C_{11}-N_7	1.402 (1.403)	1.367 (1.364)
C_{11}=O_{22}	1.229 (1.236)	1.349 (1.345)
C_{13}-N_{14}	1.365 (1.356)	1.289 (1.291)
N_{14}-H_{23}	1.011 (1.013)	-
O_{15}-H_{31}	-	0.969 (0.970)
Bond angles (°)	**Keto**	**Enol**
O_{15}-C_{11}-N_7	126 (126)	124 (125)
H_{23}-N_{14}-C_{13}	113 (114)	-
H_{31}-O_{15}-C_{11}	-	110 (111)
Hydrogen bond distances (Å)	**Keto**	**Enol**
H_{38}···O_{22}	2.187 (2.199)	-
N_8···H_{24}	2.390 (2.402)	-
N_8···H_{28}	2.478 (2.488)	-
N_{14}···H_{45}	-	2.475 (2.504)

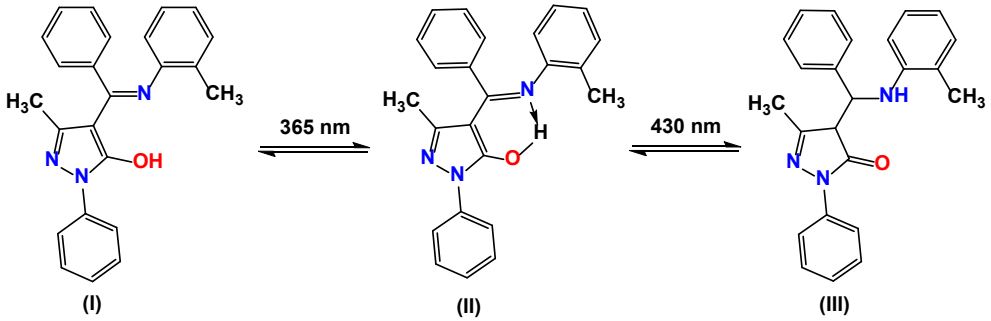

Scheme 2. Photoisomerization reaction of PMBP-2A1MB.

The *keto* tautomer's structural assignment is fully supported by its vibrational frequencies (Table 3). Aromatic C–H stretching modes are seen in the area 3086-3055 cm^{-1} [21], while the distinctive N–H stretching vibration is observed at 3452 cm^{-1} [34]. Between 3025 and 2929 cm^{-1}, aliphatic CH_3 stretching vibrations occur [35]. The *keto* form is definitively identified by a prominent and extremely intense band at 1682 cm^{-1}, which is attributed to C=O stretching [36]. An extended conjugated system is indicated by bands in the 1600-1540 cm^{-1} range, which correspond to the C–C and C–N stretching modes [35]. The strong C9–N8 vibration highlights considerable electron delocalization [32]. The N–H, C–H, and CH_3 groups' bending, wagging, and deformation vibrations are the primary sources of lower-frequency modes (1500-1300 cm^{-1}) [37].

Table 3 describes the calculate data and their relative *enol* and *keto* forms frequencies. FT-IR spectra provide clear evidence for the *enol–keto* tautomeric transformation through characteristic changes in functional group vibrations. In the initial spectrum, a broad absorption band at 3340 cm^{-1} is assigned to the intramolecularly hydrogen-bonded O–H stretching vibration, confirming the presence of the enol form stabilized by O–H···N hydrogen bonding. The band observed at 1659 cm^{-1} corresponds to the azomethine C=N stretching vibration, while the peaks in the region 1605-1543 cm^{-1} are attributed to aromatic C=C stretching. Upon photoirradiation, the disappearance of the O–H stretching band and the appearance of a strong new band at 1672 cm^{-1}, characteristic of C=O stretching, confirm the formation of the *keto* tautomer. This transformation occurs by intramolecular proton transfer from the hydroxyl oxygen to the azomethine nitrogen, resulting in the conversion of the enol form (C–OH and C=N) into the *keto* form (C=O and N–H). The observed spectral changes provide direct confirmation of the photoinduced *enol–keto* tautomerism, consistent with the mechanism proposed in Scheme 2 [37].

3.4. Mechanism of photochromism

The probable mechanism of photoisomerization is shown in Scheme 2. The photoisomerization is conversion of *enol* form (I) into *keto* form (III) via transient (II) due to the process of *intra* hydrogen binding as shown in Scheme 2. Theoretical data also support the given photoisomerization. As Table 4 summarizes the optimized bond lengths, bond angles, and hydrogen bonding parameters of the *keto* and *enol* tautomers of the compound, both in the gas phase and in methanol (values in parentheses). In the *keto* tautomer, the C_{11}=O_{22} bond length of ~1.23 Å is characteristic of a carbonyl group, while its pronounced elongation to ~1.35 Å in the enol form indicates transformation to a C–O single bond upon tautomerization. This change is accompanied by a noticeable shortening of the C_{13}–N_{14} bond in the enol tautomer, suggesting increased π-electron delocalization [38].

The C_1–N_7 and N_7–N_8 bond lengths exhibit only minor variations between the two tautomers, implying that the core molecular framework remains largely unaffected by proton transfer. The presence of N_{14}–H_{23} in the *keto* form and O_{15}–H_{31} in the *enol* form, together with their corresponding bond angles, clearly identifies the preferred protonation sites in each tautomer [39]. Intramolecular hydrogen-bond interactions are observed in both forms, with additional N–H···N hydrogen bonding stabilizing the enol tautomer. The close correspondence between the gas-phase and methanol values indicates that solvent effects lead to only slight geometrical modifications, without altering the overall structural trends of the *enol-keto* equilibrium [40].

4. Conclusions

A novel photochromic compound featuring a pyrazolone ring was synthesized. The theoretical calculations indicate that the properties of photoisomerization arise from the isomerization process that transitions from the enol form to the keto form, and the mechanism of photo isomerism attributed to intramolecular hydrogen bonds. The data obtained from cyclic voltammetry further corroborated the delocalization of π electrons within the molecules in relation to the band gap. The CV results indicate that the synthesized compound may serve as promising candidates for optoelectronic materials. The theoretical data align well with the experimental findings. The synthesized compound has potential for future applications in the construction of optoelectronic devices that respond to various stimuli, such as light or voltage. Therefore, future research will focus on evaluating the stability, reversibility, and performance of the compound under diverse environmental conditions and exploring its integration into functional optoelectronic devices. These investigations will further establish the suitability of this pyrazolone-based photochromic system for applications in smart optical switches, sensors, and other stimuli-responsive optoelectronic materials.

Disclosure statement

Conflict of interest: The authors declare that they have no conflict of interest.
Ethical approval: All ethical guidelines have been followed.

ORCID and Email

Pratima Surati
prsurati21@gmail.com
https://orcid.org/0000-0002-7977-4396

References

[1]. Irie, M. Diarylethenes for Memories and Switches. *Chem. Rev.* **2000**, *100* (5), 1685–1716.
[2]. Nitschke, P.; Jarząbek, B.; Damaceanu, M.; Bejan, A.; Chaber, P. Spectroscopic and electrochemical properties of thiophene-phenylene based Shiff-bases with alkoxy side groups, towards photovoltaic applications. *Spectrochim. Acta A: Mol. Biomol. Spec.* **2021**, *248*, 119242.
[3]. Cozzi, P. G. Metal–Salen Schiff base complexes in catalysis: practical aspects. *Chem. Soc. Rev.* **2004**, *33* (7), 410–421.
[4]. Ko, C.; Yam, V. W. Coordination Compounds with Photochromic Ligands: Ready Tunability and Visible Light-Sensitized Photochromism *Acc. Chem. Res.* **2017**, *51* (1), 149–159.
[5]. Chemes, D. M.; Alonso de Armiño, D. J.; Cutin, E. H.; Oberhammer, H.; Robles, N. L. Synthesis, characterization and vibrational studies of p-chlorosulfinylaniline. *J. Mol. Struct.* **2017**, *1127*, 191–198.
[6]. Ru, Y.; Shi, Z.; Zhang, J.; Wang, J.; Chen, B.; Huang, R.; Liu, G.; Yu, T. Recent progress of photochromic materials towards photocontrollable devices. *Mater. Chem. Front.* **2021**, *5* (21), 7737–7758.
[7]. Gentili, P. L. Chemical AI in the Limelight: The Contribution of Photochromic Materials and Oscillatory Chemical Reactions. *Advanced Optical Materials* **2025**, *13* (15), https://doi.org/10.1002/adom.202500016.
[8]. Gu, C.; Jia, A.; Zhang, Y.; Zhang, S. X. Emerging Electrochromic Materials and Devices for Future Displays. *Chem. Rev.* **2022**, *122* (18), 14679–14721.
[9]. Monk, P.; Mortimer, R.; Rosseinsky, D. Electrochromism and Electrochromic Devices. Cambridge University Press, 2007, https://doi.org/10.1017/CBO9780511550959.
[10]. Singh, R. K.; Singh, A. K. Synthesis, molecular structure, spectral analysis, natural bond order and intramolecular interactions of 2-acetylpyridine thiosemicarbazone: A combined DFT and AIM approach. *J. Mol. Struct.* **2015**, *1094*, 61–72.
[11]. Hariharan, P. C.; Pople, J. A. The influence of polarization functions on molecular orbital hydrogenation energies. *Theoret. Chim. Acta* **1973**, *28* (3), 213–222.
[12]. Liu, G.; Liu, L.; Jia, D.; Yu, K. Synthesis, Structure and Photochromic Properties of 1-Phenyl-3-Methyl-4-(4-Bromobenzal)-Pyrazolone-5 Thiosemicarbazone. *Struct. Chem.* **2005**, *16* (2), 135–140.
[13]. Wang, J.; Liu, L.; Liu, G.; Guo, J.; Jia, D. Three novel photoisomeric compounds of the 4-acyl pyrazolone derivants: Crystal structures and substituent effects on photo-isomerism in solid state. *Sci. China. Ser. B-Chem.* **2008**, *51* (7), 661–668.
[14]. Peng, B.; Liu, G.; Liu, L.; Jia, D.; Yu, K. Crystal structure and spectroscopic study on photochromism of 1-phenyl-3-methyl-4-benzal-5-pyrazolone 4-ethylthiosemicarbazone. *J. Mol. Struct.* **2004**, *692* (1-3), 217–222.
[15]. Liu, L.; Jia, D.-Z.; Ji, Y.-L.; Yu, K.-B. Crystal structure and photochromism of 1-phenyl-3-methyl-4-benzyl-5-one-pyrazole S-methyl thiosemicarbazone. *J. Mol. Struct.* **2003**, *655*, 221–227.
[16]. Saha Halder, S.; Roy, S.; Kumar Mondal, T.; Saha, R.; Sinha, C. 1-Alkyl-2-{(*O*-Thioalkyl)Phenylazo}Imidazole Complexes of Pb^{II} and Their Photochromic Property. *Zeitschrift. Anorg. Allge. Chemie* **2013**, *639* (10), 1861–1870.
[17]. Surati, P. R. Photochromic and Photoswitchable Study of Pyrazolone-Based Compound and Its Ni(II) ion Sensing Ability. *J. Anal. Chem.* **2022**, *77* (8), 1010–1014.
[18]. Irie, M.; Fukaminato, T.; Matsuda, K.; Kobatake, S. Photochromism of Diarylethene Molecules and Crystals: Memories, Switches, and Actuators. *Chem. Rev.* **2014**, *114* (24), 12174–12277.
[19]. Bléger, D.; Hecht, S. Visible-Light-Activated Molecular Switches. *Angew. Chem. Int. Ed.* **2015**, *54* (39), 11338–11349.
[20]. Altun, Y.; Köseoğlu, F. Solute-Solvent Interaction Effects on Protonation Equilibrium of Substituted N-Benzylidene-2-hydroxyanilines in Aqueous Ethanol: The Application of Factor Analysis to Solvatochromic Parameters and Protonation Equilibria. *Monatsh. Chem.* **2006**, *137* (6), 703–716.
[21]. Shah, B. A.; Surati, P. R.; Shah, A. V. Chemionics Study of Newly Synthesized Photochromic Schiff Base Compound. *Molecular. Crystals. and. Liquid. Crystals.* **2013**, *575* (1), 115–127.
[22]. Chong, D. P. Recent Advances in Density Functional Methods. *Recent. Advances. in. Computational. Chemistry.* **1995**, https://doi.org/10.1142/2914.
[23]. Turro, N. J.; Ramamurthy, V.; Scaiano, J. C. Principles of molecular photochemistry: An introduction; University Science Books: Sausalito, CA, 2009.
[24]. Mortimer, R. J. Electrochromic materials. *Chem. Soc. Rev.* **1997**, *26* (3), 147–156.
[25]. Onur, E.; Lee, J.; Aymerich-Armengol, R.; Lim, J.; Dai, Y.; Tüysüz, H.; Scheu, C.; Weidenthaler, C. Exploring the Effects of the Photochromic Response and Crystallization on the Local Structure of Noncrystalline Niobium Oxide. *ACS. Appl. Mater. Interfaces.* **2024**, *16* (19), 25136–25147.
[26]. Algi, M. P.; Cihaner, A.; Algi, F. Design, synthesis, photochromism and electrochemistry of a novel material with pendant photochromic units. *Tetrahedron* **2014**, *70* (34), 5064–5072.

[27]. Zhang, J.; Zou, Q.; Tian, H. Photochromic Materials: More Than Meets The Eye. *Advanced Materials* **2012**, *25* (3), 378–399.
[28]. Duan, C.; Cai, W.; Huang, F.; Zhang, J.; Wang, M.; Yang, T.; Zhong, C.; Gong, X.; Cao, Y. Novel Silafluorene-Based Conjugated Polymers with Pendant Acceptor Groups for High Performance Solar Cells. *Macromolecules* **2010**, *43* (12), 5262–5268.
[29]. Wu, X.; Wang, W.; Li, B.; Hou, Y.; Niu, H.; Zhang, Y.; Wang, S.; Bai, X. Synthesis and electrochromic, acidochromic properties of Schiff bases containing triphenylamine and thiophene units. *Spectrochim Acta A: Mol. Biomol. Spectr.* **2015**, *140*, 398–406.
[30]. Areephong, J.; Browne, W. R.; Katsonis, N.; Feringa, B. L. Photo- and electro-chromism of diarylethene modified ITO electrodes—towards molecular based read–write–erase information storage. *Chem. Commun.* **2006**, 3930–3932.
[31]. Castro, M. R.; Schellenberg, P.; Belsley, M.; Fonseca, A. C.; Fernandes, S. S.; Raposo, M. M. Design, synthesis and evaluation of redox, second order nonlinear optical properties and theoretical DFT studies of novel bithiophene azo dyes functionalized with thiadiazole acceptor groups. *Dyes Pigments* **2012**, *95* (2), 392–399.
[32]. Guo, J.; Ren, T.; Zhang, J.; Li, G.; Li, W.; Yang, L. Crystal structure characterization as well as theoretical study of spectroscopic properties of novel Schiff bases containing pyrazole group. *Spectrochim. Acta A: Mol. Biomol. Spectr.* **2012**, *95*, 135–142.
[33]. Jacquemin, D.; Wathelet, V.; Perpète, E. A.; Adamo, C. Extensive TD-DFT Benchmark: Singlet-Excited States of Organic Molecules. *J. Chem. Theory. Comput.* **2009**, *5* (9), 2420–2435.
[34]. Chai, H.; Liu, G.; Liu, L.; Jia, D. Synthesis and spectroscopic study on photochromism of a new thiosemicarbazone compound containing pyrazolone. *Spectrochim. Acta A: Mol. Biomol. Spectr.* **2005**, *61* (11-12), 2590–2594.
[35]. Liu, H.; Guo, J.; Jia, D.; Guo, M.; Liu, L.; Wu, D. Fluorescence modulation of a pyrazolone dye in the solid state based on energy transfer. *New. J. Chem.* **2015**, *39* (12), 9866–9871.
[36]. Surati, P. R.; Shah, B. A. Photochromic and molecular switching behaviour of Schiff base-containing pyrazolone ring. *Chemical Papers* **2015**, *69* (2), https://doi.org/10.1515/chempap-2015-0021.
[37]. Guo, Y.; Liu, G.; Liu, L.; Jia, D. A theoretical study of the photochromic mechanism of a novel photochromic compound: 1-phenyl-3-methyl-4-(4-bromobenzal) pyrazolone-5 thiosemicarbazone. *J. Mol. Struct: THEOCHEM* **2004**, *712* (1-3), 223–231.
[38]. Hadjoudis, E.; Mavridis, I. M. Photochromism and thermochromism of Schiff bases in the solid state: structural aspects. *Chem. Soc. Rev.* **2004**, *33* (9), 579–588 https://doi.org/10.1039/B303644H.
[39]. Amimoto, K.; Kawato, T. Photochromism of organic compounds in the crystal state. *J. Photochem. Photobio. C: Photochem. Rev.* **2005**, *6* (4), 207–226.
[40]. Surati, P. R. Photochromic and Electrochromic Study of Schiff Bases Containing Pyrazolone and Anthracene Unit. *J. Struct. Chem.* **2023**, *64* (6), 984–994.